Asian Journal of Chemistry; *Vol. 38, No. 5 (2026), 1267-1278*

ASIAN JOURNAL OF CHEMISTRY

https://doi.org/10.14233/ajchem.2026.35582

Kinetic, Equilibrium and Thermodynamic Study of Chlorantraniliprole Removal from Water using Zr-UiO-66

CHETNA KHOKHAR[1,*], SUSHIL AHLAWAT[1], ANUSHREE JATRANA[1], REENA CHAUHAN[1] and NISHA KUMARI[2]

[1]Department of Chemistry, College of Basic Sciences and Humanities, Chaudhary Charan Singh Haryana Agricultural University, Hisar-125004, India

[2]Department of Biochemistry, College of Basic Sciences and Humanities, Chaudhary Charan Singh Haryana Agricultural University, Hisar-125004, India

*Corresponding author: E-mail: ckhokhar28@gmail.com

Received: 8 January 2026 *Accepted*: 31 March 2026 *Published online*: 4 May 2026 AJC-22352

UiO-66, a Zr-based metal organic framework exhibited a BET surface area (S_{BET}) of 843.41 $m^2 g^{-1}$, with pore size and total pore volume 1.71 nm and 0.52 $cm^3 g^{-1}$, respectively and showed a characteristic Type I N_2 adsorption-desorption isotherm. The material had an average particle size of 958 nm and a negative zeta potential *i.e.* -30.12 mV at pH 7, indicating the negative polarity, facilitating π–π interactions and weak hydrophobic interactions with chlorantraniliprole. The adsorption of chlorantraniliprole on UiO-66 followed a favourable monolayer mechanism as described by the Langmuir isotherm and the process was endothermic and chemisorptive, consistent with the pseudo-second-order kinetic model. Thermodynamic parameters (ΔH^o = 20.50 kJ mol^{-1}; ΔS^o = 78.9 kJ $mol^{-1} K^{-1}$) and negative ΔG^o values (-0.77 to -1.66 kJ mol^{-1}) indicated spontaneous adsorption. Under optimised conditions, UiO-66 achieved 86.5% removal of chlorantraniliprole (20 mg L^{-1}). The MOF maintained performance over four regeneration cycles using DMF washing and heating (80 ºC).

Keywords: Adsorption, Chlorantraniliprole, Desorption, Equilibrium, Thermodynamic studies.

INTRODUCTION

The increasing contamination of aquatic systems by pesticide residues poses a serious threat to environmental sustainability and public health. Water is indispensable for life and global health and development depend on access to clean water resources [1]. Among emerging contaminants, pesticides are frequently detected in surface and groundwater due to their extensive agricultural use, environmental persistence and mobility, leading to adverse ecological and toxicological effects even at trace concentrations [2]. Consequently, developing efficient and reliable treatment technologies for removing pesticides from water is essential. Several approaches have been developed, including adsorption, microbial degradation [3], photocatalysis [4], Fenton reaction [5], ozonation [6], membrane separation [7], nanofiltration [8], electrochemical degradation [9] and phytoremediation [10]. Among these methods, adsorption has gained particular attention due to its operational simplicity, high efficiency and minimal secondary pollution.

Recently, metal organic frameworks (MOFs) have attracted considerable attention as advanced adsorbents due to their exceptionally high surface area, tunable porosity and structural versatility [11]. Among various MOFs, Zr-based UiO-66 stands out because of its outstanding hydrolytic stability and robustness under aqueous conditions, making it particularly suitable for water treatment applications [12]. While UiO-66 has been previously studied for the adsorption of organic contaminants, most reports focus on modified UiO-66 or model pollutants such as dyes and pharmaceuticals [13]. In contrast, systematic investigations on the adsorption behaviour of agricultural pesticides using pristine UiO-66 remain limited, particularly for chlorantraniliprole removal. The present study therefore evaluates the adsorption performance of conventional UiO-66 under environmentally relevant conditions, including kinetic, isotherm, thermodynamic and pH-dependent analyses, to better understand the adsorption mechanism. Moreover, the baseline studies using pristine materials provide an important reference for assessing the effectiveness of future modified UiO-66 systems.

Chlorantraniliprole, a widely used anthranilic diamide insecticide, has been increasing reported in aquatic environments, raising concerns regarding its persistence and ecological risks [14]. Adsorption capacity depends strongly on several experimental factors, including the physicochemical properties of the target pollutant (polarity, molecular size, pK_a), solution pH, initial concentration and adsorption conditions [15]. Pristine UiO-66 often exhibits moderate adsorption capacities, while significantly higher capacities are typically achieved only after structural modification or composite formation [16]. Therefore, the primary aim of this work is not to maximize adsorption capacity through material modification, but to systematically evaluate the adsorption behaviour and mechanism of pesticide removal using UiO-66. Establishing such baseline performance is essential for understanding adsorption mechanisms and for benchmarking future modified materials. In this work, the adsorption performance of Zr-UiO-66 for chlorantraniliprole removal from water is investigated through detailed kinetic, equilibrium and thermodynamic analyses. The study provides mechanistic insights into the adsorption process and highlights the potential of Zr-UiO-66 as an efficient adsorbent for pesticide-contaminated water treatment.

EXPERIMENTAL

Certified reference material (CRM) of chlorantraniliprole (98.6% purity, CAS No. 500008-45-7) was obtained from Sigma-Aldrich GmbH, Switzerland. Zirconium tetrachloride ($ZrCl_4$), terephthalic acid (benzene-1,4-dicarboxylic acid, BDC), dimethylformamide (DMF, HPLC grade) and chloroform were procured from Sigma-Aldrich Pvt. Ltd. All chemicals were of analytical or HPLC grade and used as received. Ultrapure water (18.2 MΩ cm) was used throughout the adsorption study.

Synthesis of UiO-66: UiO-66 was synthesised *via* facile solvothermal method following Rahmawati *et al.* [17]. Zirconium tetrachloride (0.7 g) and benzenedicarboxylic acid (BDC, 0.5 g) were dissolved in 30 mL of DMF and stirred at 50 ºC for 30 min to obtain a homogeneous precursor solution. The mixture was transferred to a Teflon-lined autoclave and heated at 140 ºC for 6 h. After gradual cooling to ambient temperature, the resultant was filtered, washed with DMF and left for 24 h, then rinsed with chloroform twice and vacuum-dried at 80 ºC for 24 h to yield crystalline UiO-66 (yield: 94.17%). The product was obtained as a fine, fluffy white powder with zirconium chloride considered the limiting reagent for the reaction:

$$ZrCl_4 + H_2BDC + H_2O \longrightarrow Zr_6O_4(OH)_4(BDC)_6 + 4HCl$$

Characterisation: The surface morphology of synthesised UiO-66 was examined using JSM-761FPlus field emission scanning electron microscope (FE-SEM) along with its elemental composition with the help of energy dispersive X-ray spectrometer (EDX) combined with FE-SEM chamber. The functional group identification was carried out by FT-IR using Thermo Scientific Spectrometer (Nicolet-50) in the 4000-400 cm^{-1} region. The surface area, average pore volume and the pore size distribution and the total pore volume were examined using a Quantachrome IQ-XR-XR (2stat.) BET analyzer by degassing 100-120 mg samples at 120 ºC prior to N_2 adsorption/desorption analysis, density functional theory (DFT) model and Barrett-Joyner-Halenda (BJH) method, respectively. The particle size and zeta-potential of UiO-66 was determined using a microtrac particle size analyzer (Nanotrac Wave II, Microtrac Retsch GmbH, Germany).

Batch studies: Batch experiments were conducted to optimize different key parameters (pH, adsorbent dose, pesticide concentration, contact time and temperature). A stock solution of chlorantraniliprole (1000 mg/L) was prepared using distilled water as solvent and working concentrations ranging from 10 to 100 mg/L were obtained through serial dilution. Calibration standards were analysed using UV-Vis double-beam spectrophotometer (Shimadzu) and absorbance was recorded at the maximum wavelength of 260 nm. Prior to adsorption experiments, the adsorbent (UiO-66) was activated by overnight evacuation in a vacuum oven at 120 ºC and subsequently stored in a desiccator. The effect of pH on adsorption using 20 mg/L chlorantraniliprole solutions adjusted to pH 2 to 9 with 0.1 M HCl and 0.1 M NaOH. For each experiment, 20 mL of solution was transferred to a glass vial and UiO-66 was added at a dosage of 0.02 g/L. The mixtures were agitated on an orbital shaker at 800 rpm for 60 min at 30 ºC, followed by centrifugation and filtration. The residual chlorantraniliprole concentration was determined using UV-Vis spectrophotometry. Adsorbent dose optimisation was conducted by varying the UiO-66 dosage from 0.02, 0.04, 0.06, 0.08, 0.1, 0.2 and 0.4 g/L using 20 mg/L chlorantraniliprole solutions at the optimised pH. The effects of contact time and temperature were investigated by withdrawing samples at regular intervals (10 to 80 min) at three temperatures (303 K, 313 K and 323 K) under constant agitation (800 rpm). Initial concentration studies were performed using chlorantraniliprole solutions of 20 to 70 mg/L while maintaining optimised adsorbent dose, pH, temperature and contact time. All the experiments were carried out in triplicate and mean values were reported. The percentage removal efficiency and adsorption capacity were calculated using eqns. 1 and 2:

$$\text{Removal efficiency (\%)} = \frac{\text{Initial}_{\text{conc.}} - \text{Final}_{\text{conc.}}}{\text{Initial}_{\text{conc.}}} \times 100 \quad (1)$$

$$\text{Adsorption capacity} = \frac{(\text{Initial}_{\text{conc.}} - \text{Final}_{\text{conc.}}) \times \text{Volume}}{\text{Mass of adsorbent}} \quad (2)$$

Point of zero charge (pH_{PZC}) analysis: UiO-66 (20 mg) was added to a flask containing 20 mL of NaCl 0.1 M at eight different pH values (pH = 2, 3, 4, 5, 6, 7, 8, 9). The solutions were stirred for 20 min and maintained stable during 24 h. After 24 h the mixture was centrifuged and then filtered. The final pH was measured by a pH meter. The curve was plotted *via* ΔpH = pH (initial) – pH (final) *versus* pH (initial) and the pH_{pzc} was calculated at ΔpH = 0 [18].

Adsorption studies

Adsorption isotherms: Adsorption isotherms offer essential insights into the optimal utilisation of adsorbents by describing the equilibrium distribution of insecticide molecules between the aqueous and solid phases [19], thereby enabling effective adsorbent design and application. In this study, the adsorption behaviour of chlorantraniliprole onto UiO-66 was estimated using four isotherm models *i.e.* Freundlich, Langmuir, Temkin and Dubinin-Radushkevich (D-R) by varying the initial chlorantraniliprole concentration from 20 to 70 mg/L while maintaining a constant UiO-66 dosage.

Adsorption kinetics: Adsorption kinetic studies elucidate the rate, mechanism and time required to attain equilibrium. In this study, the adsorption kinetics of chlorantraniliprole on UiO-66 were evaluated using four kinetic models *i.e.* pseudo-first order, pseudo-second order, intraparticle diffusion and Elovich model [20] over contact times ranging from 10 to 80 min.

Thermodynamic studies: The thermodynamic behaviour of chlorantraniliprole adsorption onto UiO-66 was evaluated at different temperatures to determine the changes in entropy (ΔS), enthalpy (ΔH) and Gibbs free energy (ΔG). These parameters were calculated using van't Hoff equation by plotting ln K_d *versus* 1/T, where the slope and intercept of the linear fit correspond to ΔH and ΔS, respectively [21,22].

$$\ln K_d = \frac{\Delta S}{R} - \frac{\Delta H}{RT} \quad (3)$$

here K_d denotes the mass-weighted partition coefficient between the solid and liquid phases and was calculated using eqn. 4:

$$K_d = \frac{C_o - C_t}{C_t} \times \frac{V}{M} \quad (4)$$

where C_o represents initial concentration (mg/L) and C_t represents the concentration of insecticide at contact time t and ΔG was determined for each temperature using eqn. 5:

$$\Delta G = \Delta H - T\Delta S \quad (5)$$

RESULTS AND DISCUSSION

FT-IR of UiO-66: FT-IR spectrum of UiO-66 (Fig. 1) confirms its successful synthesis from $ZrCl_4$ and BDC. The disappearance of the Zr-Cl stretching band 547 cm^{-1} indicates complete consumption of $ZrCl_4$. The carboxyl C=O stretching band of free BDC at 1669 cm^{-1} shifts to asymmetric and symmetric carboxylate vibrations at 1560 and 1406 cm^{-1}, respectively, indicating coordination of BDC with Zr^{4+}. The emergence of a Zr-O stretching band at 690 cm^{-1} further confirmed the formation of the Zr-O-C framework, is consistent with Gurmessa *et al.* [23] and Cliffe *et al.* [24]. A slight shift in the C-O stretching band and the retention of the aromatic C=C stretching peak at 1530 cm^{-1} indicate the successful MOF formation while preserving the benzene ring structure.

Fig. 2 illustrates the FTIR spectra of UiO-66 before and after chlorantraniliprole adsorption. The presence of O-H stretching (3377 cm^{-1}) suggests adsorbed water or hydroxyl groups on the framework (UiO-66). In case of chlorantraniliprole,

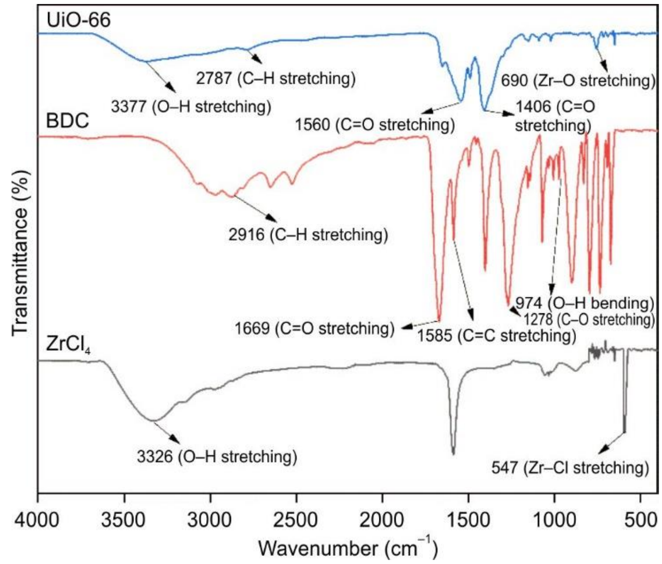

Fig. 1. FTIR spectra of $ZrCl_4$, BDC and synthesised UiO-66

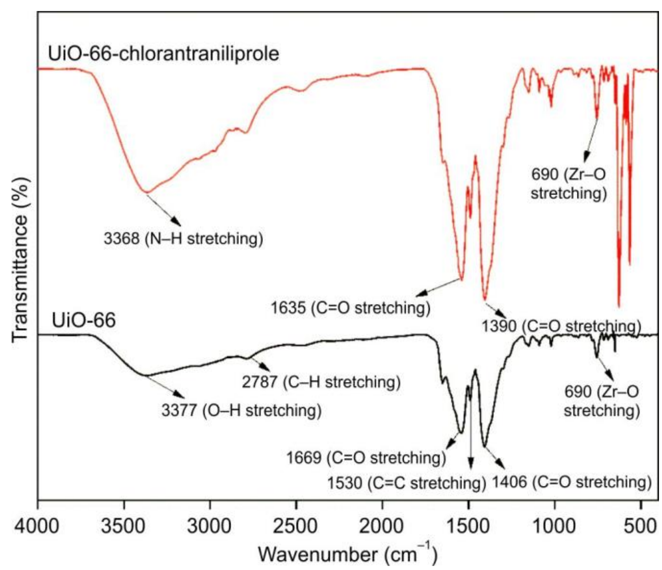

Fig. 2. FTIR spectrum of UiO-66 after adsorption

N–H stretching peak appears at 3368 cm^{-1} indicating the presence of amine groups. Chlorantraniliprole also displays amide C=O stretching (1635 cm^{-1}) and C-Cl stretching (636 cm^{-1}), which are absent in UiO-66, distinguishing its molecular structure. The observed shifts provide insight into the binding mechanisms between UiO-66 and chlorantraniliprole, confirming the successful adsorption and potential applications in environmental remediation.

BET studies: The compiled textural parameters, including BET surface area (S_{BET}), total pore volume, pore size and micropore volume of the synthesised UiO-66, are shown in Table-1. N_2 adsorption-desorption analysis exhibits a Type I isotherm, confirming the microporous nature of the material

TABLE-1
SURFACE AREA, TOTAL PORE VOLUME, PORE SIZE AND PORE VOLUME DETERMINED USING BET ANALYSIS

Adsorbent	Surface area (S_{BET}) (m^2/g)	Average pore size (Å)	Total pore volume (cc/g)	Pore radius (nm)
UiO-66	843.41	1.71	0.52	0.85

(Fig. 3). The synthesised UiO-66 shows a S_{BET} of 843.41 m^2/g and a micropore volume of 0.52 cc/g. These results are consistent with those reported by Mohammed *et al.* [25] for surface area in the literature.

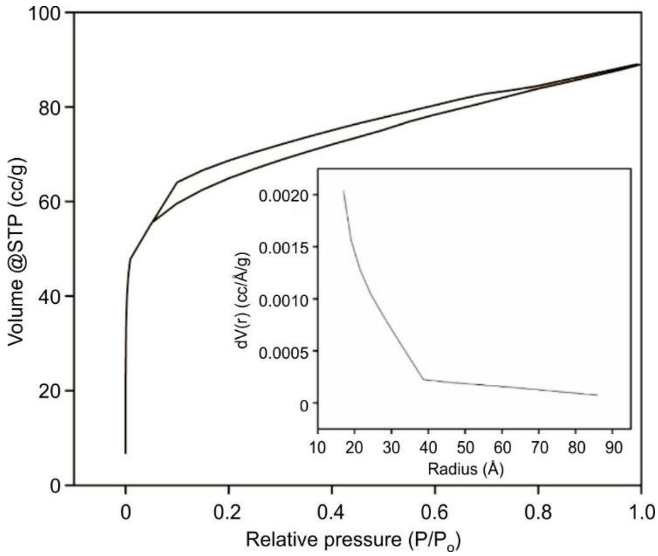

Fig. 3. N_2 adsorption-desorption isotherm and pore size distribution of UiO-66

Pore surface area of UiO-66: The synthesised UiO-66 exhibits an average particle size of 958 nm (Fig. 4). At pH 7, it shows a negative zeta potential, indicating a negatively charged surface, attributed to the presence of carboxylate (COO^-) groups from the BDC linker.

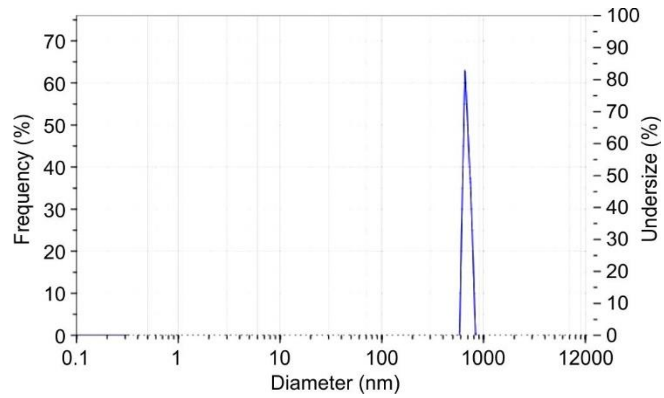

Fig. 4. Particle size analyzer (PSA) result of synthesised UiO-66

Morphological studies: FE-SEM images of synthesized UiO-66 show well-defined polyhedral crystals with smooth surfaces and sharp edges, indicating good crystallinity (Fig 5). The particles exhibit slight agglomeration, which is typical for zirconium-based MOFs. After adsorption, the morphology becomes rougher with irregular deposits and clustered structures on the surface (Fig 6). The polyhedral features appear less distinct, suggesting attachment of adsorbate species. However, the structure remains intact, confirming successful adsorption without the disintegration of the UiO-66 framework.

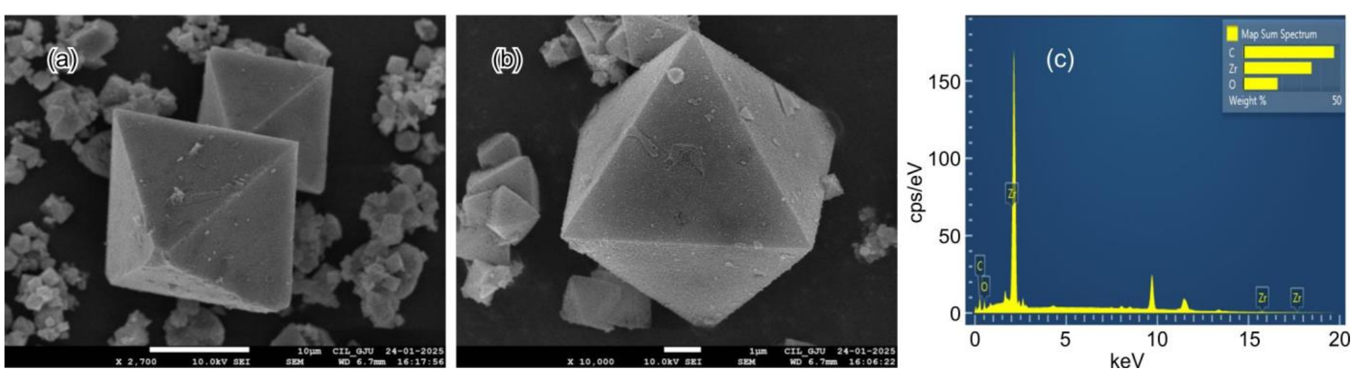

Fig. 5. FE-SEM micrographs (a,b) and EDS spectrum (c) of synthesised UiO-66

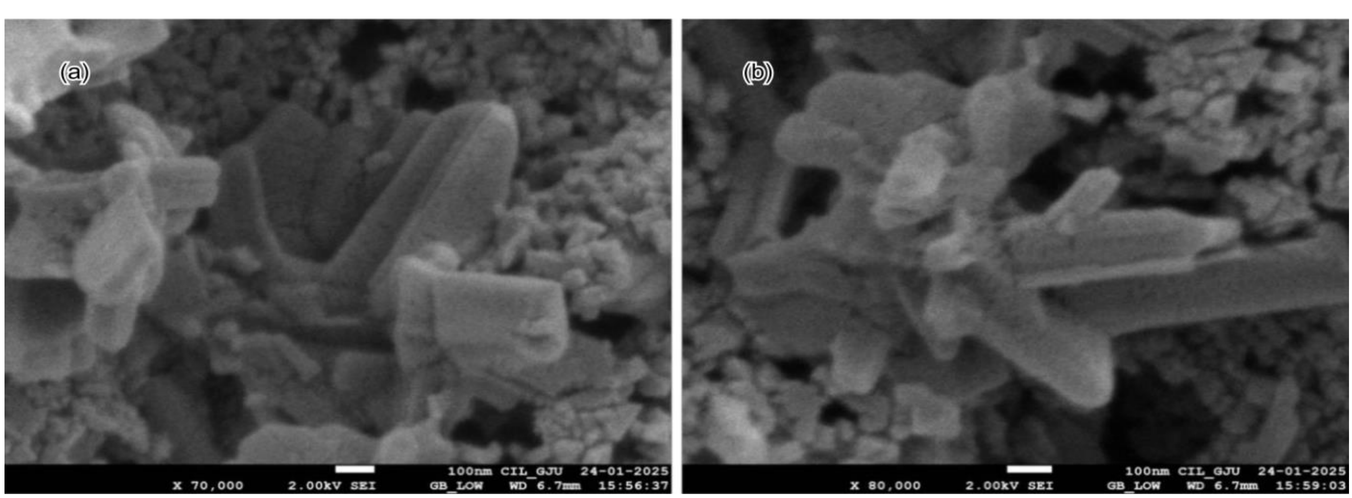

Fig. 6. FE-SEM micrographs of UiO-66 after adsorption

The EDX analysis confirms the presence of carbon, oxygen and zirconium with percentages of 46.88%, 17.86% and 35.26%, respectively (Fig. 5c). These findings are in line with the findings of Ly *et al.* [26] and Rajendran *et al.* [27].

Optimisation of adsorption parameters

Effect of pH: The pH of chlorantraniliprole solutions was optimised by adjusting it from 2 to 10. In this, the removal efficiency increased with pH and reached a maximum of 57.5% at pH 4. Further increases in pH led to a decline in removal efficiency, as illustrated in Fig. 7a. The most probable reason is that at lower pH, the functional groups such as -COOH and -OH present on the UiO-66 surface becomes protonated, thus increasing the affinity for interaction of partial negative ions of insecticides which will eventually leads to the weak electrostatic interactions as suggested by Rajendran *et al.* [27], who also suggested that at pH 3 UiO-66 experiences maximum removal efficiency.

Effect of dose: The optimum UiO-66 dose was determined by varying the adsorbent concentration from 0.02 to 0.4 g/L. The maximum removal efficiency of 69% was attained at 0.08 g/L, as shown in Fig. 7b. These results can be attributed to the increase in total surface area and the availability of more active sites on UiO-66, which collectively enhance adsorption. However, beyond an optimum adsorbent dose, further addition leads to particle agglomeration, reducing the effective surface area and causing a decline in removal efficiency [22,28,29].

Effect of concentration: The influence of initial chlorantraniliprole concentration on adsorption was examined over a range of 20 to 70 mg/L. The results showed a decrease in percentage removal with increasing concentration, with the maximum removal efficiency of 71% achieved at 20 mg/L (Fig. 7c). Similar trends were observed by Gurmessa *et al.* [23], who reported a decrease in removal efficiency of malathion and 2,4-D from aqueous solution using UiO-66 with increasing concentration.

Effect of contact time and temperature: Adsorption experiments were performed to examine the influence of contact time and temperature at 303, 313 and 323 K over a time interval of 10 to 80 min. The maximum removal of 79.5% was achieved at 313 K within 50 min, while 75% removal was

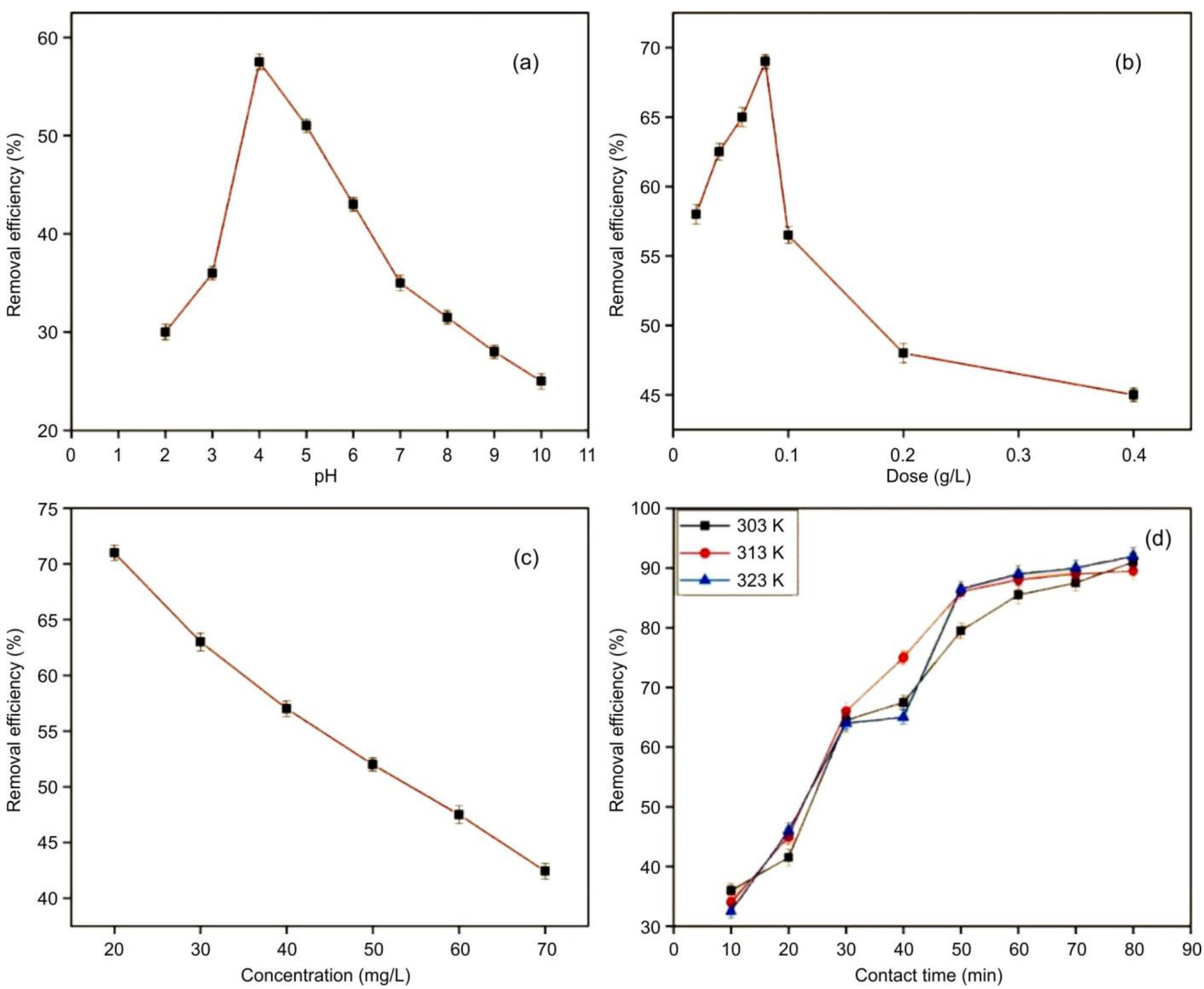

Fig. 7. Effect of (a) pH, (b) dose (g/L), (c) concentration (mg/L), (d) contact time (min) *vs.* removal efficiency (%)

observed at the same temperature after 40 min. The highest removal efficiency (86.5%) was obtained at 323 K with contact time of 50 min, as shown in Fig. 7d. These findings are consistent with the studies reported by Mirazaei *et al.* [30] and ElHussein *et al.* [31].

Point of zero charge (pH_{PZC}) analysis: The point of zero charge (pH_{PZC}) of the synthesised UiO-66 was found to be 3.8 which is below 4 (Fig. 8), indicating that surface of the UiO-66 becomes negatively charged at pH > pH_{PZC} [32]. Therefore, within the studied pH range of 2-9, the material gradually shifts from slightly positive to negative surface charge as the pH increases. The zeta potential measurements further confirmed this behaviour, showing negative zeta potential values at neutral pH, which indicates that the surface of the UiO-66 is predominantly negatively charged under environmental conditions [33]. Consequently, at neutral pH, the surface of UiO-66 carries a negative charge. Since, the studied pesticide exists in the cationic form, mild electrostatic attraction occurs between the positively charged chlorantraniliprole and the negatively charged UiO-66 surface, which enhances the adsorption process.

Adsorption isotherm studies: Adsorption isotherms are used to study the relationship between the amount of pollutant adsorbed onto an adsorbent and its concentration in the surrounding solution. Table-2 compares the coefficients of determination (R^2) obtained from different adsorption isotherm

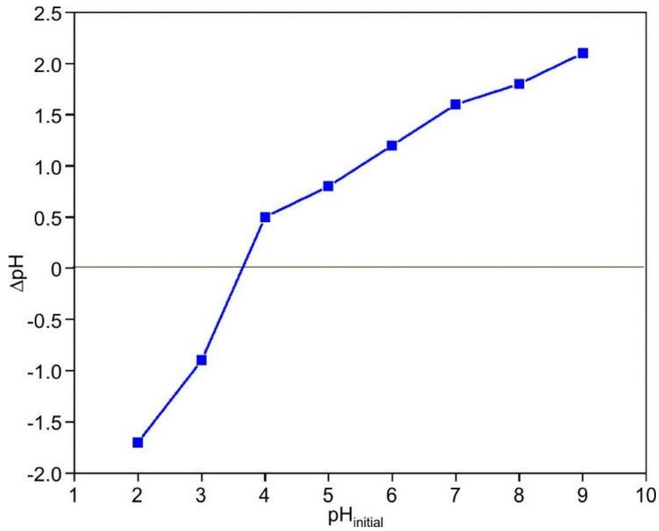

Fig. 8. pH_{PZC} of adsorption chlorantraniliprole on UiO-66

models in both linear (Fig. 9) and non-linear (Fig. 10) forms for chlorantraniliprole adsorption onto UiO-66. The Langmuir and Temkin models showed the best fit to the experimental data, with R^2 values closer to unity than those of Freundlich and D-R models and with the lower chi square (χ^2) values. The good agreement of the experimental data with Langmuir isotherm suggests a homogeneous distribution of identical

TABLE-2
DETAILS OF ADSORPTION ISOTHERM MODELS AND THEIR PARAMETERS FOR CHLORANTRANILIPROLE ADSORPTION ON UiO-66

Adsorption isotherm model	Form	Expression	Plot	Parameters	R^2
Langmuir isotherm	Linear	$\frac{1}{Q_e} = \frac{1}{K_L \times Q_{max}} \times \frac{1}{C_e} + \frac{1}{Q_{max}}$	$1/Q_e$ *vs.* $1/C_e$	$Q_{max, cal}$ (mg/g) = 8.928 K_L (L/g) = 0.111 R_L = 0.310 χ^2 = 0.046	0.989
	Non-linear	$Q_e = \frac{Q_{max} \times K_L \times C_e}{(1 + K_L \times C_e)}$	Q_e *vs.* C_e	$Q_{max, cal}$ (mg/g) = 9.288 K_L (L/g) = 0.098 R_L = 0.337 χ^2 = 0.037	0.991
Freundlich isotherm	Linear	$\log Q_e = \log K_f + \frac{1}{n} \log C_e$	log Q_e *vs.* log C_e	K_F (L/g) = 1.828 1/n = 0.391 χ^2 = 0.073	0.981
	Non-linear	$Q_e = K_f \times (C_e)^{1/n}$	Q_e *vs.* C_e	K_F (L/g) = 1.931 1/n = 0.373 χ^2 = 0.064	0.982
Temkin isotherm	Linear	$Q_e = \frac{RT}{b} \ln K_T + \frac{RT}{b} \ln C_e$	ln Q_e *vs.* ln C_e	b_T (g kJ/mg mol) = 0.932 K_T (L/g) = 0.936 χ^2 = 0.065	0.982
	Non-linear	$Q_e = \frac{RT}{b} \ln (K_T C_e)$	Q_e *vs.* C_e	b_T (g kJ/mg mol) = 0.710 K_T (L/g) = 0.924 χ^2 = 0.038	0.989
Dubinin-Raudshkevich isotherm	Linear	$\ln Q_e = \ln Q_{max}^{DR} - K_{DR} \varepsilon^2$	ln Q_e *vs.* ε^2	Q_{max}^{DR} (mg/g) = 16.28 K_{DR} (mol²/K² J²) = 0.006 E (kJ/mol) = 9.174 χ^2 = 0.087	0.837
	Non-linear	$Q_e = Q_{max}^{DR} e^{-K_{DR}\varepsilon^2}$	Q_e *vs.* ε^2	Q_{max}^{DR} (mg/g) = 14.42 K_{DR} (mol²/K² J²) = 0.003 E (kJ/mol) = 12.99 χ^2 = 0.039	0.988

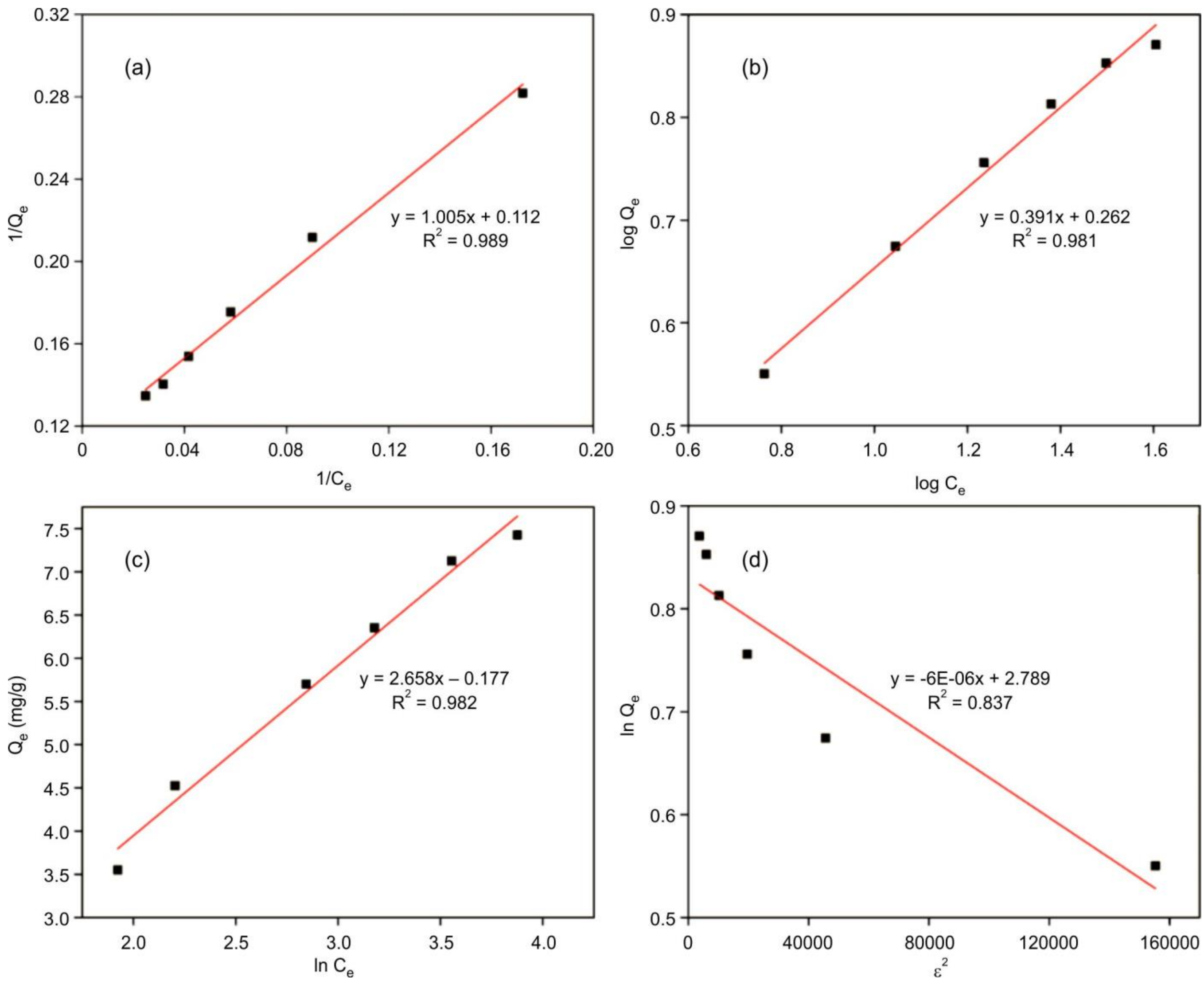

Fig. 9. Linearly fitted isotherm models of (a) Langmuir (b) Freundlich (c) Temkin and (d) Dubinin-Raudshkevich

active sites on the UiO-66 surface, with monolayer adsorption of chlorantraniliprole occurring at discrete sites without intermolecular interactions.

The separation factor (R_L) values for chlorantraniliprole adsorption (0.310 for linear and 0.337 for non-linear) lie between 0 and 1, indicating favourable adsorption, which is further supported by the negative Gibbs free energy values [34]. To contextualize the adsorption performance of UiO-66, the maximum adsorption capacity (Q_{max}) obtained in this study was compared with literature values reported for adsorption of various contaminants on UiO-66 (Table-3). Therefore, the results indicate that pristine UiO-66 can effectively adsorb chlorantraniliprole and holds promise for application in water purification systems.

Adsorption kinetic studies: Table-4 presents the kinetic parameters and corresponding R^2 values for different kinetic models in both linear (Fig. 11) and non-linear (Fig. 12) form describing chlorantraniliprole adsorption onto UiO-66. Among these, the pseudo second order model exhibited the highest R^2 values at all three temperatures, indicating the best agreement with the experimental data.

TABLE-3
COMPARATIVE DATA OF ADSORPTION CAPACITIES OF UiO-66 MATERIALS REPORTED FOR ADSORPTION

Adsorbent	Target contaminant	Maximum adsorption capacity (Q_{max}) (mg/g)	Isotherm model	Ref.
UiO-66	Chlorantraniliprole	9.28	Langmuir	Present study
UiO-66	Ni^{2+}, Fe^{3+}	6.8, 14.1	Langmuir	[35]
UiO-66	Phenol, metronidazole, rhodamine B	2.06, 8.54, 56.4	Adams-Bohart	[36]
UiO-66	Methylene blue, methyl orange	13.2, 84.8	Langmuir	[37]
UiO-66	Diazinon	4.4	Langmuir	[38]

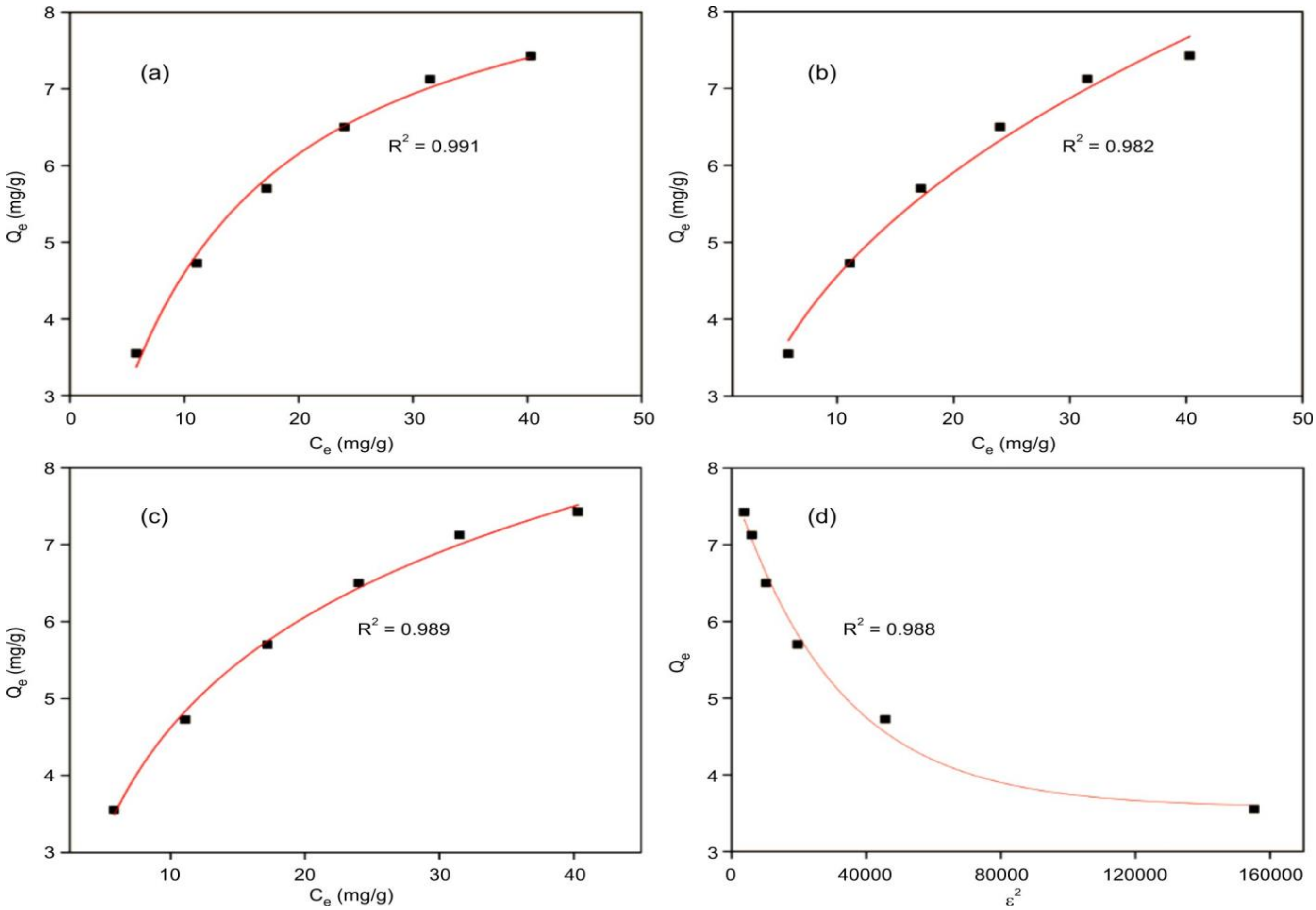

Fig. 10. Non-linearly fitted isotherm models of (a) Langmuir (b) Freundlich (c) Temkin and (d) Dubinin-Raudshkevich

TABLE-4
DETAILS OF KINETIC MODELS AND THEIR PARAMETERS FOR ADSORPTION OF CHLORANTRANILIPROLE ON UiO-66

Kinetic models	Form	Expression	Plot	Temp. (K)	Kinetic parameters	R^2
Pseudo first order	Linear	$\ln(Q_t - Q_e) = \ln Q_e - K_1 t$	ln (Q_e – Q_t) *vs.* t	303	$Q_{e,\ exp}$ = 5.00; $Q_{e,\ cal}$ = 4.636; K_1 = -0.029	0.981
				313	$Q_{e,\ exp}$ = 4.50; $Q_{e,\ cal}$ = 8.498; K_1 = -0.072	0.976
				323	$Q_{e,\ exp}$ = 5.00; $Q_{e,\ cal}$ = 4.892; K_1 = -0.033	0.937
	Non-linear	$Q_t = Q_e(1 - e^{-K_1 t})$	Q_t *vs.* t	303	$Q_{e,\ exp}$ = 5.00; $Q_{e,\ cal}$ = 4.838; K_1 = 0.033	0.949
				313	$Q_{e,\ exp}$ = 4.50; $Q_{e,\ cal}$ = 4.837; K_1 = 0.037	0.972
				323	$Q_{e,\ exp}$ = 5.00; $Q_{e,\ cal}$ = 4.324; K_1 = 0.428	0.350
Pseudo second order	Linear	$\frac{t}{Q_t} = \frac{1}{K_2 \times Q_e^2} + \frac{t}{Q_e}$	t/Q_t *vs.* t	303	$Q_{e,\ exp}$ = 5.00; $Q_{e,\ cal}$ = 6.251; K_2 = 0.004	0.997
				313	$Q_{e,\ exp}$ = 4.50; $Q_{e,\ cal}$ = 6.329; K_2 = 0.005	0.984
				323	$Q_{e,\ exp}$ = 5.00; $Q_{e,\ cal}$ = 6.756; K_2 = 0.006	0.979
	Non-linear	$Q_t = \frac{Q_e^2 K_2 t}{1 + K_2 t Q_e}$	Q_t *vs.* t	303	$Q_{e,\ exp}$ = 5.00; $Q_{e,\ cal}$ = 5.337; K_2 = 4.660	0.960
				313	$Q_{e,\ exp}$ = 4.50; $Q_{e,\ cal}$ = 4.885; K_2 = 4.749	0.967
				323	$Q_{e,\ exp}$ = 5.00; $Q_{e,\ cal}$ = 5.086; K_2 = 4.905	0.979
Intraparticle diffusion model	Linear	$Q_t = K_i t^{0.5} + I$	Q_t *vs.* $t^{0.5}$	303	K_{diff} = 0.125; C = 0.550	0.950
				313	K_{diff} = 0.203; C = 0.523	0.916
				323	K_{diff} = 0.232; C = 0.516	0.942
	Non-linear	$Q_t = K_i t^{0.5}$	Q_t *vs.* $t^{0.5}$	303	K_{diff} = 0.156; C = 1.465	0.737
				313	K_{diff} = 0.291; C = 1.451	0.732
				323	K_{diff} = 0.293; C = 1.436	0.706
Elovich model	Linear	$Q_t = \frac{1}{\beta}\ln(\alpha.\beta) + \frac{1}{\beta}\ln t$	Q_t *vs.* ln t	303	α = 115.094; β = 0.687	0.945
				313	α = 135.242; β = 0.765	0.953
				323	α = 156.181; β = 0.838	0.947
	Non-linear	$Q_t = \frac{1}{\beta}\ln(\alpha.\beta.t + 1)$	Q_t *vs.* t	303	α = 34.252; β = 0.530	0.958
				313	α = 96.282; β = 0.542	0.949
				323	α = 116.237; β = 0.583	0.953

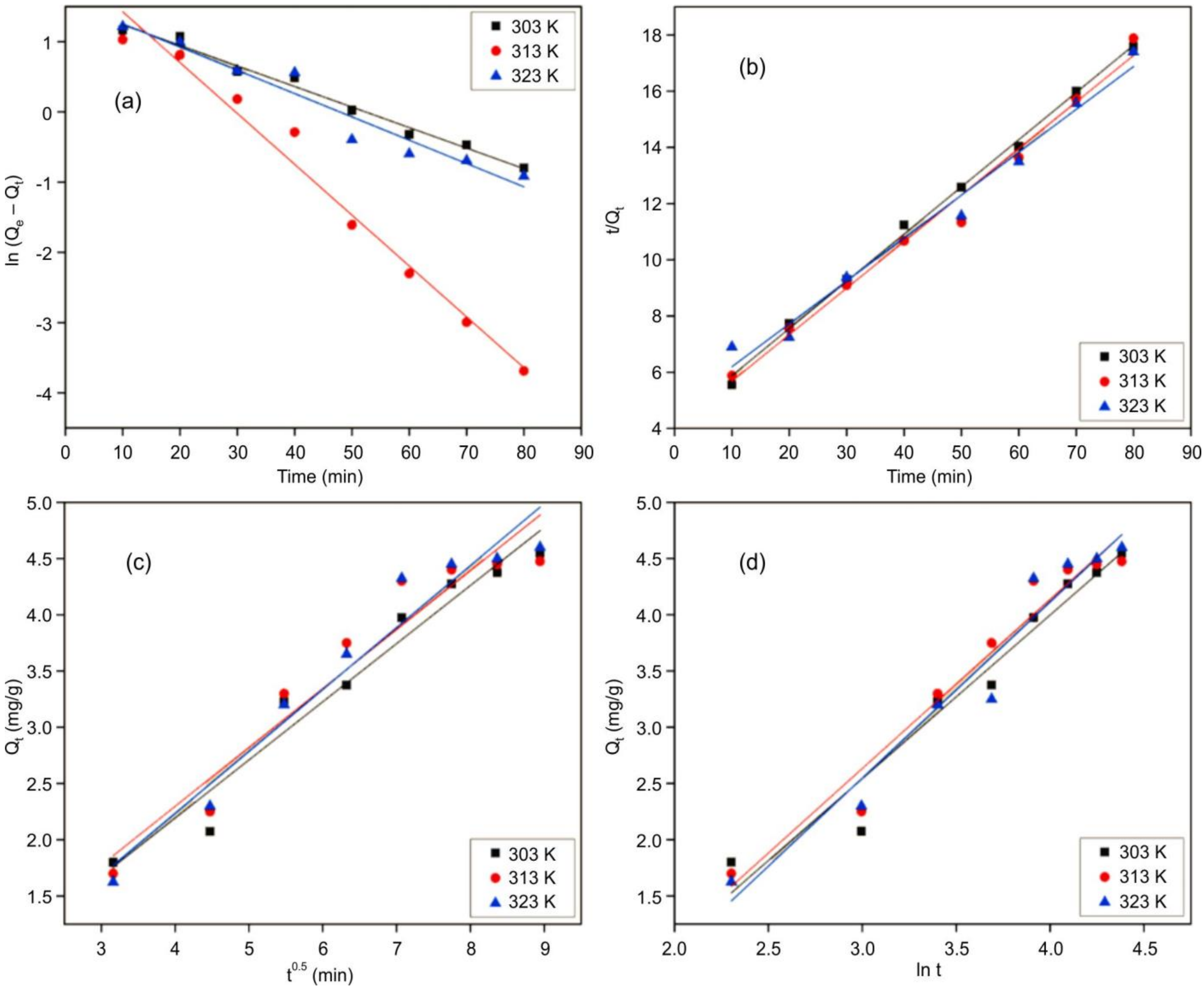

Fig. 11. Linearly fitted kinetic models of (a) Pseudo-first order (b) Pseudo-second order (c) Intraparticle diffusion and (d) Elovich

The conformity of the pseudo-second order model highlights chemisorption as the dominant driving force for chlorantraniliprole uptake on synthesised UiO-66. An increase in the rate constant (K_2) from 303 to 323 K reflects the temperature-dependent and thermally activated behaviour of the process. In line with Le Chatelier's principle, this behaviour confirms that chlorantraniliprole adsorption onto UiO-66 proceeds *via* an endothermic mechanism [22,39].

Thermodynamic studies: The thermodynamic nature and feasibility of chlorantraniliprole adsorption onto UiO-66 were assessed using van't Hoff plot (Fig. 13). The thermodynamic parameters (ΔG, ΔH and ΔS) are summarised in Table-5. The Gibbs free energy (ΔG) values at 303, 313 and 323 K were -0.77, -1.30 and -1.66 kJ mol^{-1}, respectively, confirming that the adsorption process is spontaneous and thermodynamically favourable [21]. The observed increase in the distribution coefficient (K_d) with rising temperature further indicates enhanced adsorption efficiency at higher temperatures. The positive ΔH values demonstrate the endothermic nature of the process, while the positive ΔS values reflect a strong affinity between UiO-66 and chlorantraniliprole, along with increased randomness at the solid-solution interface arising from the structural reorganisation of both the adsorbent and adsorbate [40,41].

Reusability of UiO-66: The reusability of UiO-66 was evaluated over successive adsorption-desorption cycles for

TABLE-5
THERMODYNAMIC PARAMETERS FOR ADSORPTION OF CHLORANTRANILIPROLE ON UiO-66

Insecticide	Temperature (K)	ΔG (kJ/mol)	ΔS (kJ/mol K)	ΔH (kJ/mol)	R^2
	303	-0.77			
Chlorantraniliprole	313	-1.30	78.9	20.5	0.986
	323	-1.66			

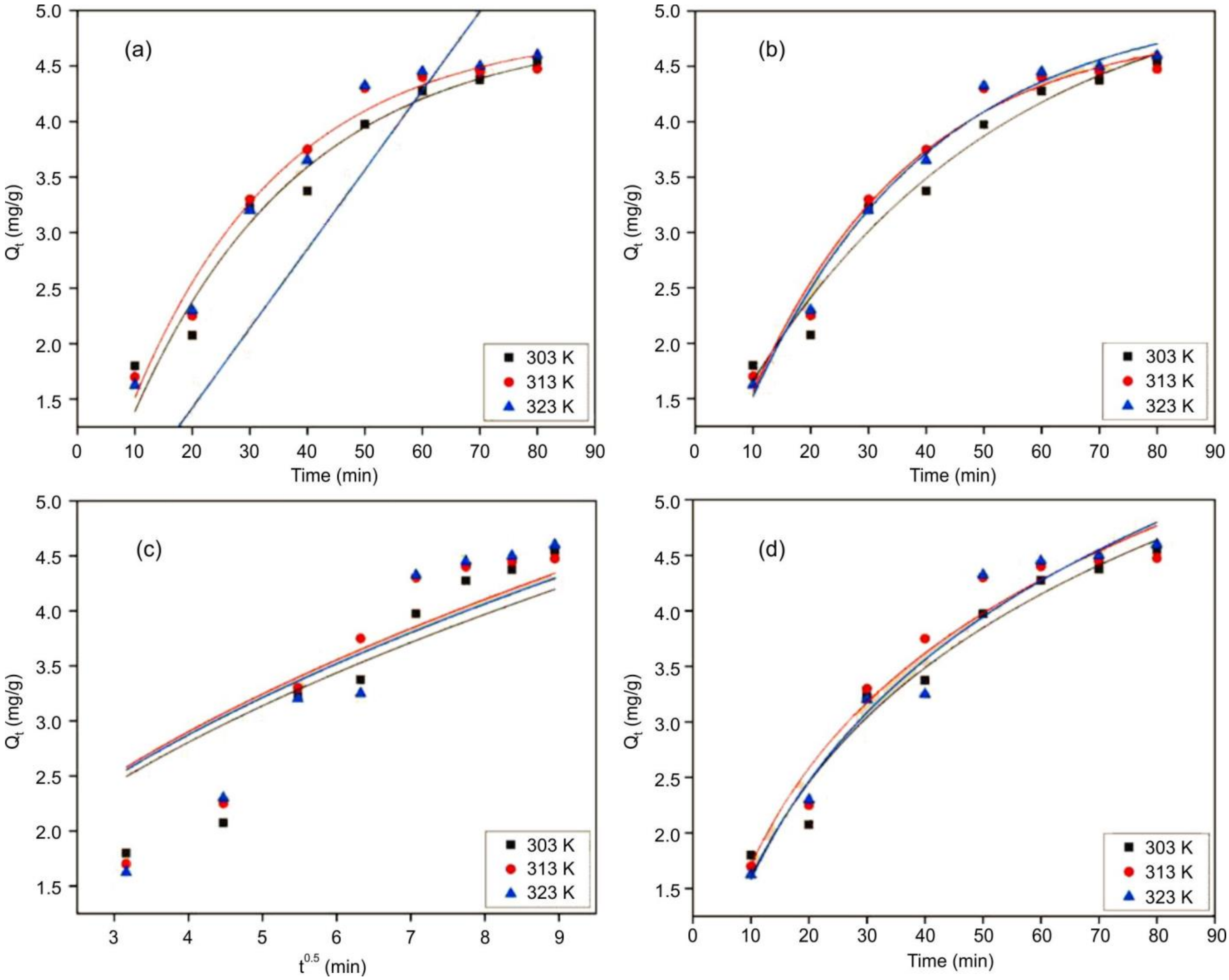

Fig. 12. Non-linearly fitted kinetic models of (a) Pseudo-first order (b) Pseudo-second order (c) Intraparticle diffusion and (d) Elovich

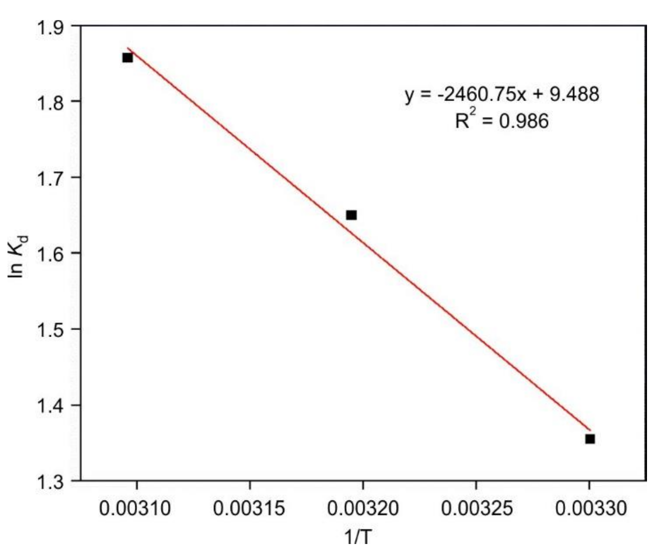

Fig. 13. Plot of ln K_d *vs.* 1/T for chlorantraniliprole adsorption on UiO-66

chlorantraniliprole removal. After each cycle, the adsorbent was separated from the solution, washed 2 to 3 times with DMF to eliminate residual contaminants, vacuum dried at 80 ºC before reuse. UiO-66 was regenerated and reused for up to four cycles, exhibiting only a 2.6% reduction in adsorption efficiency while retaining its structural integrity, as shown in Fig. 14. These results demonstrate the excellent recyclability and durability of UiO-66 for repeated removal of chlorantraniliprole removal and agreed with the previous report [42].

Plausible adsorption mechanism: The adsorption mechanism of an adsorbate onto MOF active sites may involve various types of interactions including π-π interactions, electrostatic interactions, complex formation, hydrogen boding, acid-base interactions and hydrophobic interactions [43]. The octahedral structure of UiO-66 is composed of zircomium ($Zr_6O_4(OH)_4$) clusters connected by 1,2-benzene dicarboxylic acid (BDC) linkers and exhibits a negatively charged surface at neutral pH. Chlorantraniliprole, which contains electron-deficient group such as amide (–$CONH_2$), can interact electrostatically with the positively charged Zr^{4+} sites on UiO-66 (Fig. 15). The aromatic rings can interact with the benzene ring present in synthesised UiO-66 *via* π-π interaction, these findings are in alignment with those reported by Gurmessa *et al.* [23].

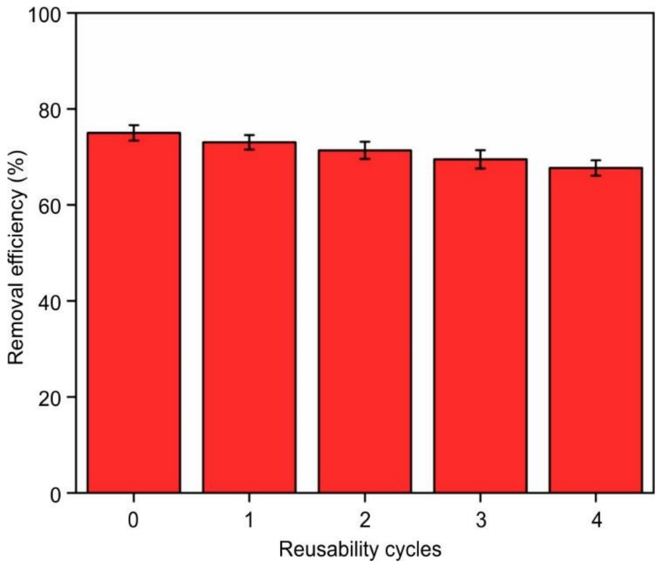

Fig. 14. Reusability data of UiO-66

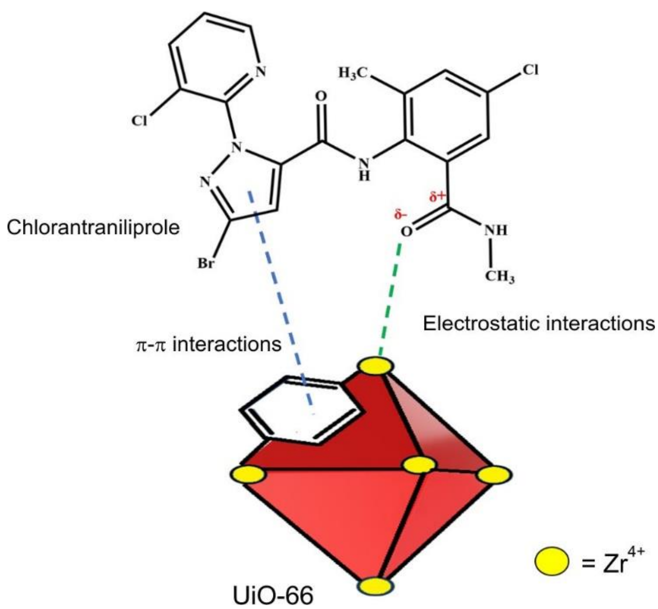

Fig. 15. Mechanism of adsorption of chlorantraniliprole on UiO-66

Conclusion

In this study, it is concluded that Zr-UiO-66 synthesised *via* the solvothermal method exhibited high surface area, microporosity and excellent aqueous stability, making it an effective adsorbent for chlorantraniliprole removal from water. Adsorption performance was strongly governed by solution pH, adsorbent dose, contact time, temperature and initial concentration, with a maximum removal efficiency of 86.5% under optimised conditions. Equilibrium data were best described by the Langmuir isotherm, indicating favourable monolayer adsorption on a homogeneous surface. Kinetic studies revealed that the pseudo second order model provided the best fit, confirming chemisorption as the rate-limiting step. Thermodynamic analysis showed negative ΔG values, demonstrating spontaneous adsorption, while positive ΔH and ΔS values confirmed an endothermic process accompanied by increased interfacial disorder. UiO-66 retained the structural integrity and adsorption efficiency over four regeneration cycles, highlighting its recyclability and operational stability. The adsorption experiments in this study were performed in a single-solute system to understand the intrinsic interaction between chlorantraniliprole and UiO-66. However, natural water matrices contain competing ions and dissolved organic matter that may influence adsorption behavior. Therefore, further investigations using real water samples or multicomponent systems are recommended to evaluate the practical applicability of the material.

ACKNOWLEDGEMENTS

The authors gratefully acknowledge Chaudhary Charan Singh Haryana Agricultural University, Hisar for providing the necessary laboratory facilities, instrumental and technical assistance and research support to carry out this work.

CONFLICT OF INTEREST

The authors declare that there is no conflict of interests regarding the publication of this article.

DECLARATION OF AI-ASSISTED TECHNOLOGIES

During the preparation of this manuscript, the authors used an AI-assisted tool(s) to improve the language. The authors reviewed and edited the content and take full responsibility for the published work.

REFERENCES

1. J. Li, H. Wang, X. Yuan, J. Zhang and J.W. Chew, *Coord. Chem. Rev.*, **404**, 213116 (2020); https://doi.org/10.1016/j.ccr.2019.213116
2. M.M.H. Mondol and S.H. Jhung, *Chem. Eng. J.*, **421**, 129688 (2021); https://doi.org/10.1016/j.cej.2021.129688
3. A. Mojiri, J.L. Zhou, B. Robinson, A. Ohashi, N. Ozaki, T. Kindaichi, H. Farraji and M. Vakili, *Chemosphere*, **253**, 126646 (2020); https://doi.org/10.1016/j.chemosphere.2020.126646
4. S. Ahmed, M.G. Rasul, R. Brown and M.A. Hashib, *J. Environ. Manage.*, **92**, 311 (2011); https://doi.org/10.1016/j.jenvman.2010.08.028
5. R. Li, C. Yang, H. Chen, G. Zeng, G. Yu and J. Guo, *J. Hazard. Mater.*, **167**, 1028 (2009); https://doi.org/10.1016/j.jhazmat.2009.01.090
6. J. Wang and H. Chen, *Sci. Total Environ.*, **704**, 135249 (2020); https://doi.org/10.1016/j.scitotenv.2019.135249
7. M.Q. Seah, Z.C. Ng, G.S. Lai, W.J. Lau, M.A. Al-Ghouti, N.H. Alias, and A.F. Ismail, *Chemosphere*, **356**, 141960 (2024); https://doi.org/10.1016/j.chemosphere.2024.141960
8. J.B. Moreira, T.D. Santos, M. Zaparoli, A.C.A. de Almeida, J.A.V. Costa and M.G. de Morais, *Appl. Sci.*, **12**, 8352 (2022); https://doi.org/10.3390/app12168352
9. A. Dube, S.J. Malode, M.A. Alshehri and N.P. Shetti, *J. Environ. Chem. Eng.*, **12**, 114916 (2024); https://doi.org/10.1016/j.jece.2024.114916
10. A.U. Khan, A.N. Khan, A. Waris, M. Ilyas and D. Zamel, *Open Life Sci.*, **17**, 488 (2022); https://doi.org/10.1515/biol-2022-0056
11. X. Zhang, X. Tian, N. Wu, S. Zhao, Y. Qin, F. Pan, S. Yue, X. Ma, J. Qiao, W. Xu, W. Liu, J. Liu, M. Zhao, K. Ostrikov and Z. Zeng, *Sci. Adv.*, **10**, eadl6498 (2024); https://doi.org/10.1126/sciadv.adl6498
12. M. Kadhom, M. Al-Furaiji, S. Salih, M.A. Al-Obaidi, G.H. Abdullah and N. Albayati, *J. Water Process Eng.*, **51**, 103402 (2023); https://doi.org/10.1016/j.jwpe.2022.103402

13. X. Zhao, Y. Wang, D. Li, X. Bu and P. Feng, *Adv. Mater.*, **30**, 1705189 (2018); https://doi.org/10.1002/adma.201705189
14. Y. Xiao, C. Chen, Y. Wu, J. Wang, Y. Yin, J. Chen, X. Huang, P. Qi and B. Zheng, *Micropor. Mesopor. Mater.*, **324**, 111272 (2021); https://doi.org/10.1016/j.micromeso.2021.111272
15. S. Satyam and S. Patra, *Heliyon*, **10**, e29573 (2024); https://doi.org/10.1016/j.heliyon.2024.e29573
16. S. Xu, L. Wang, F. Wang, S. Fu, W. Meng, G. He, W. Cao and W. Zhang, *J. Water Process Eng.*, **75**, 108017 (2025); https://doi.org/10.1016/j.jwpe.2025.108017
17. I.D. Rahmawati, R. Ediati and D. Prasetyoko, *IPTEK J. Proc. Series*, **1**, 42 (2014); https://doi.org/10.12962%2Fj23546026.y2014i1.417
18. N. Priyadarshini, K. Kumar Das, S. Mansingh and K. Parida, *Results Chem.*, **4**, 100450 (2022); https://doi.org/10.1016/j.rechem.2022.100450
19. F. Khakbaz, M. Mahani and M. Yoosefian, *Anal. Methods Environ. Chem. J.*, **5**, 24 (2022); https://doi.org/10.24200/amecj.v5.i02.175
20. H. Bukhari, *J. Saudi Chem. Soc.*, **28**, 101949 (2024); https://doi.org/10.1016/j.jscs.2024.101949
21. S.H. Alrefaee, M. Aljohani, K. Alkhamis, F. Shaaban, M.G. El-Desouky, A.A. El-Bindary and M.A. El-Bindary, *J. Mol. Liq.*, **384**, 122206 (2023); https://doi.org/10.1016/j.molliq.2023.122206
22. A. Jamali, F. Shemirani and A. Morsali, *J. Ind. Eng. Chem.*, **80**, 83 (2019); https://doi.org/10.1016/j.jiec.2019.07.034
23. B.K. Gurmessa, A.M. Taddesse and E. Teju, *Environ. Pollut. Bioavail.*, **35**, 2222910 (2023); https://doi.org/10.1080/26395940.2023.2222910
24. M.J. Cliffe, W. Wan, X. Zou, P.A. Chater, A.K. Kleppe, M.G. Tucker, H. Wilhelm, N.P. Funnell, F. Coudert and A.L. Goodwin, *Nat. Commun.*, **5**, 4176 (2014); https://doi.org/10.1038/ncomms5176
25. M.M. Mohammed, A.A. El-Fadl, A.A. Abu-Sehly and M. Rashad, *J. Solid State Electrochem.*, **29**, 2801 (2025); https://doi.org/10.1007/s10008-024-06190-0
26. N.H. Ly, N.B. Nguyen, N.H. Tran, T.T.H. Hoang, S.W. Joo, Y. Vasseghian, H. Kamyab, S. Chelliapan and J. J. Klemeš, *J. Cleaner Product.*, **402**, 136809 (2023); https://doi.org/10.1016/j.jclepro.2023.136809
27. H.K. Rajendran, M. Das, R. Chandrasekar, M.A. Deen, B. Murugan, S. Narayanasamy and L. Sahoo, *Environ. Sci. Pollut. Res. Int.*, **30**, 114264 (2023); https://doi.org/10.1007/s11356-023-30296-z
28. P. Kuwer, A. Yadav and P.K. Labhasetwar, *Water Sci. Technol.*, **84**, 2288 (2021); https://doi.org/10.2166/wst.2021.452
29. F. Sharifipour, S. Hojati, A. Landi and A. Faz Cano, *Int. J. Environ. Res.*, **9**, 1001 (2015).
30. K. Mirzaei, E. Jafarpour, A. Shojaei, S.S. Khasraghi and P. Jafarpour, *Appl. Surf. Sci.*, **618**, 156531 (2023); https://doi.org/10.1016/j.apsusc.2023.156531
31. E.A.A. ElHussein, S. Şahin and S.S. Bayazit, *J. Environ. Chem. Eng.*, **8**, 103898 (2020); https://doi.org/10.1016/j.jece.2020.103898
32. H.T. Dinh, N.T. Tran and D.X. Trinh, *J. Anal. Methods Chem.*, **2021**, 5512174 (2021); https://doi.org/10.1155/2021/5512174
33. I. Skans, M. Mnguni and P.N. Nomngongo, *Anal. Sci. Adv.*, **6**, e70023 (2025); https://doi.org/10.1002/ansa.70023
34. S. Santaeufemia, E. Torres, R. Mera and J. Abalde, *J. Hazard. Mater.*, **320**, 315 (2016); https://doi.org/10.1016/j.jhazmat.2016.08.042
35. L. Zhai, X. Zheng, M. Liu, X. Wang, W. Li, X. Zhu, A. Yuan, Y. Xu and P. Song, *Inorg. Chem. Commun.*, **154**, 110937 (2023); https://doi.org/10.1016/j.inoche.2023.110937
36. S. Jiang, Y. Lyu, J. Zhang, X. Zhang, M. Yuan, Z. Zhang, G. Jin, B. He, W. Xiong and H. Yi, *J. Environ. Chem. Eng.*, **12**, 111951 (2024); https://doi.org/10.1016/j.jece.2024.111951
37. J. Qiu, Y. Feng, X. Zhang, M. Jia and J. Yao, *J. Colloid Interface Sci.*, **499**, 151 (2017); https://doi.org/10.1016/j.jcis.2017.03.101
38. V. Ashouri, K. Adib, M.R. Nasrabadi and M. Ghalkhani, *J. Mol. Struct.*, **1240**, 130607 (2021); https://doi.org/10.1016/j.molstruc.2021.130607
39. F. Ahmadijokani, R. Mohammadkhani, S. Ahmadipouya, A. Shokrgozar, M. Rezakazemi, H. Molavi, T.M. Aminabhavi and M. Arjmand, *Chem. Eng. J.*, **399**, 125346 (2020); https://doi.org/10.1016/j.cej.2020.125346
40. V. Vimonses, S. Lei, B. Jin, C.W. Chow and C. Saint, *Chem. Eng. J.*, **148**, 354 (2009); https://doi.org/10.1016/j.cej.2008.09.009
41. Y. Sun, M. Chen, H. Liu, Y. Zhu, D. Wang and M. Yan, *Appl. Surf. Sci.*, **525**, 146614 (2020); https://doi.org/10.1016/j.apsusc.2020.146614
42. L. Gnanasekaran, R. Hemamalini, R. Saravanan, K. Ravichandran, F. Gracia, S. Agarwal and V.K. Gupta, *J. Photochem. Photobiol. B*, **173**, 43 (2017); https://doi.org/10.1016/j.jphotobiol.2017.05.027
43. N.A. Khan, Z. Hasan and S. H. Jhung, *J. Hazard. Mater.*, **244**, 444 (2013); https://doi.org/10.1016/j.jhazmat.2012.11.011